Gamma/X-Ray Linear Pushbroom Stereo for 3D Cargo Inspection

Zhigang Zhu[*ab], Yu-Chi Hu[bc]
[a]Department of Computer Science, The City College of New York, New York, NY 10031
[b]Department of Computer Science, The CUNY Graduate Center, New York, NY 10016
[c]Department of Medical Physics, Memorial Sloan-Kettering Cancer Center, NY 10021
* Email: zhu@cs.ccny.cuny.edu

ABSTRACT

For evaluating the contents of trucks, containers, cargo, and passenger vehicles by a non-intrusive gamma-ray or X-ray imaging system to determine the possible presence of contraband, three-dimensional (3D) measurements could provide more information than 2D measurements. In this paper, a linear pushbroom scanning model is built for such a commonly used gamma-ray or x-ray cargo inspection system. Accurate 3D measurements of the objects inside a cargo can be obtained by using two such scanning systems with different scanning angles to construct a pushbroom stereo system. A simple but robust calibration method is proposed to find the important parameters of the linear pushbroom sensors. Then, a fast and automated stereo matching algorithm based on free-form deformable registration is developed to obtain 3D measurements of the objects under inspection. A user interface is designed for 3D visualization of the objects in interests. Experimental results of sensor calibration, stereo matching, 3D measurements and visualization of a 3D cargo container and the objects inside, are presented.

Keywords: Pushbroom imaging, automatic 3D measurements, cargo inspection, homeland security

1. INTRODUCTION

With the ongoing development of international trade, cargo inspection becomes more and more important. Quite a few X-ray or gamma(γ)-ray cargo inspection systems have been put into practical uses[5,6,7,15]. In this paper, a non-intrusive gamma-ray imaging system[15] will be used as an example to describe our research work. This system produces gamma-ray radiographic images, and has been used for the evaluation of the contents of trucks, containers, cargo, and passenger vehicles to determine the possible presence of many types of contraband. In the past, however, cargo inspection systems have only had two-dimensional capabilities, and human operators made most of the measurements. But if we could build an accurate geometry model for the gamma-ray imaging system, which turns out to be a linear pushbroom scanning sensor[3], accurate three-dimensional (3D) measurements of objects inside a cargo container can be obtained when two such scanning systems with different scanning angles are used to construct a *linear pushbroom stereo system*. The 3D measurements add more value to today's cargo inspection techniques, as indicated in some online reports[5,6,7].

Pushbroom images (or mosaics, when generated from video sequences) with parallel-perspective projections are very suitable for such surveillance and/or security applications where the motion of the camera has a dominant translational direction. Examples include satellite pushbroom imaging[3], airborne video surveillance[19,20], 3D reconstruction for image-based rendering[1], road scene representations[17,18], under-vehicle inspection[2,10], and 3D measurements of industrial parts by an X-ray scanning system[4,12]. A pushbroom image/mosaic is a *parallel-perspective* image, which has parallel projection in the direction of the camera's motion and perspective projection in the direction perpendicular to that motion. A pair of pushbroom stereo images/mosaics can be used for both 3D viewing and 3D reconstruction when they are obtained from two different oblique viewing angles. An advantageous feature of the pushbroom stereo is that depth resolution is independent of depth[1,19]. This advantage can be further explained when the pushbroom stereo images are generated from a video sequence[19,20]. Since a fixed angle between the two sets of parallel viewing rays is selected for

generating the stereo mosaics, for any point in the left mosaic searching for the match point in the right mosaic means virtually finding an original frame in which this matched pair has a fixed disparity and an adaptive baseline, depending on the depth of the point. Therefore, better depth resolution could be achieved than with perspective stereo or the recently developed multi-perspective stereo with circular projection[9,13,14], given the same image resolution. We note that multi-perspective stereo with circular projection that is based on wide-baseline line cameras can achieve quite accurate depth resolution for far-range airborne scenes[9]. However in such a configuration, depth resolution is still proportional to the square of depth, therefore depth accuracy varies for the cargo inspection case with large depth variations. In addition, the circular motion that is required is not the best form for scanning long cargo containers.

In this paper, issues on 3D measurements using a linear pushbroom stereo system are studied for gamma-ray cargo inspection[15]. The closest work to ours is the x-ray metrology for industrial quality assurance[4,12]. However, to our knowledge, our paper presents the first piece of work in using linear pushbroom stereo for 3D gamma-ray or X-ray inspection of large cargo containers, with fast and fully-automated 3D measurements. This paper uses the gamma-ray scanning images provided by the Science Applications International Corporation (SAIC)[15]. However, the algorithms developed in this paper can be used for pushbroom images acquired by X-ray or other scanning approaches as well.

This paper is organized as follows. Section 2 introduces the geometry of the pushbroom scanning sensor model. In Section 3, the geometry of the pushbroom stereo system is developed. Then in Section 4, a calibration method is proposed to find the important parameters of the sensor model. In Section 5, a fast and automated stereo matching algorithm is developed considering both the radiographic and geometric properties of gamma-ray stereo images. A user interface is designed to visualize the 3D measurements of objects in interests. Finally, in Section 6, we conclude our work and discuss a few future directions in both research and applications.

2. γ-RAY LINEAR PUSHBROOM SENSOR MODEL

The system diagram of the gamma-ray cargo inspection system is shown at the bottom-left corner of Figure 1. A 1D detector array of 256 NaI-PMT probes counts the gamma-ray photons passing through the vehicle/cargo under inspection from a gamma-ray point source. Either the vehicle/cargo or the gamma-ray system (the source and the detector) moves in a straight line in order to obtain a 2D scanning of gamma-ray images.

The geometry of the system is shown in Figure 1 (right). The 1D detector array geometry can be modeled by the well-known perspective projection camera $X_cY_cZ_c$ with the optical center at the location of gamma-ray source, and the 1D detector array in the vertical direction v and at a distance f along the optical axis Z_c (i.e., f is the focal length in pixels). Note that in the figure the image is drawn between the objects and the optical center for easy illustration. The scanning begins when the optical center of the sensor is at location $T = (T_x, T_y, T_z)$ in the world coordinate system o-xyz. The angle between the optical axis (TZ_c) of the sensor and the oz axis of the world coordinate is θ. We assume there are no tilt and roll angles between the two coordinate systems. The sensor moves at a constant speed S (feet per scan) in the direction of the x-axis, so the velocity vector represented in the camera coordinate system $X_cY_cZ_c$ is $V= (V_x,V_y,V_z)= (S\cos\theta, 0, S\sin\theta)$. The center of the linear image in the v direction is defined by a vertical offset p_v. Putting all of these into the linear pushbroom projection equation formulated by Gupta & Hartley (1997)[3], we have the relationship between a 3D point (x,y,z) in the world coordinate system and its image point (u,v) as

$$\begin{pmatrix} u \\ wv \\ w \end{pmatrix} = \begin{pmatrix} 1 & 0 & 0 \\ 0 & f & p_v \\ 0 & 0 & 1 \end{pmatrix} \begin{pmatrix} \frac{1}{Vx} & 0 & 0 \\ -\frac{Vy}{Vx} & 1 & 0 \\ -\frac{Vz}{Vx} & 0 & 1 \end{pmatrix} \begin{pmatrix} \cos\theta & 0 & -\sin\theta \\ 0 & 1 & 0 \\ \sin\theta & 0 & \cos\theta \end{pmatrix} \left(\begin{pmatrix} x \\ y \\ z \end{pmatrix} - \begin{pmatrix} Tx \\ Ty \\ Tz \end{pmatrix} \right)$$

This linear pushbroom equation leads to the following two simpler equations

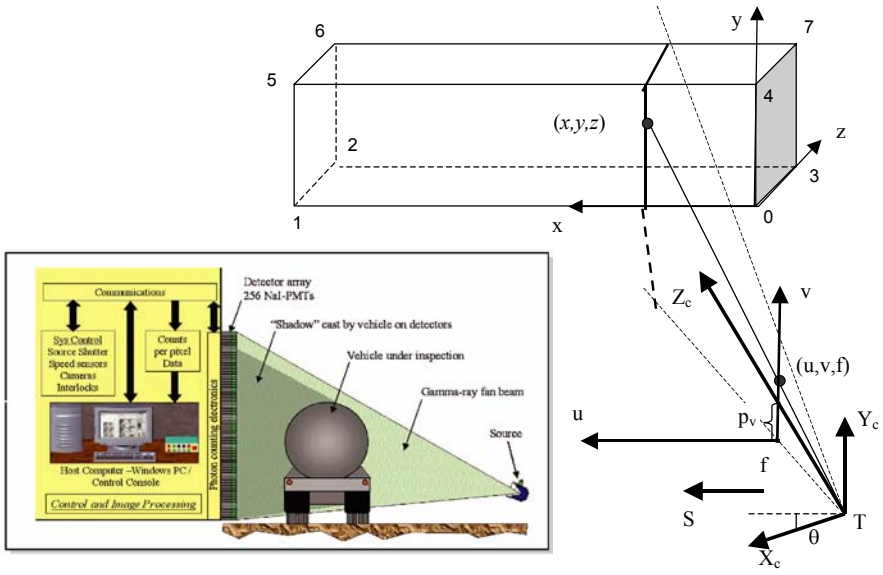

Figure 1. Linear pushbroom sensor model. A gamma-ray cargo inspection system (Courtesy SAIC, San Diego, CA, USA) that can be modeled by linear pushbroom geometry is show in the bottom-left corner of the figure.

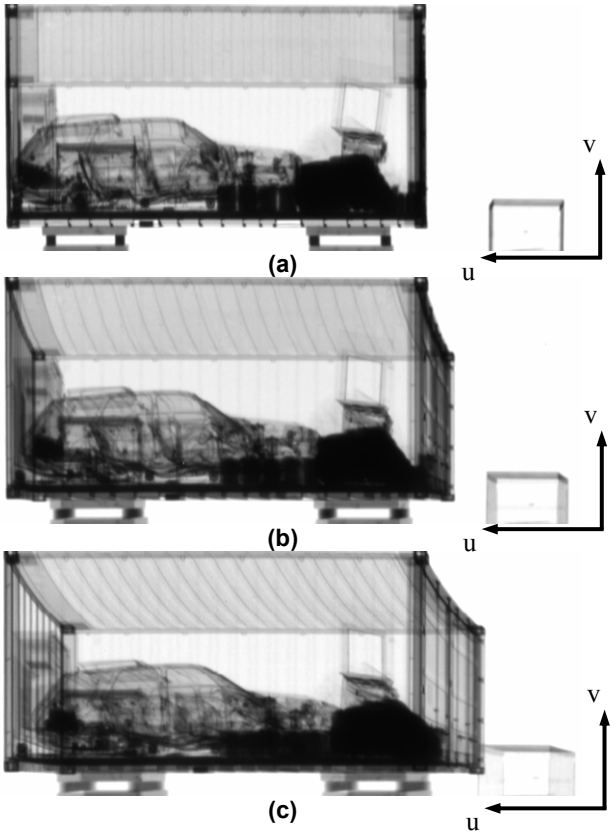

Figure 2. Real gamma-ray images with three different scanning angles (a) zero (b) ten and (c) twenty degrees (Courtesy SAIC, San Diego, CA, USA). Each image has a size of 621x256 pixels, i.e., 621 scans of the 256-pixel linear images. The stereo visual displacements, particularly the back surface of the cargo container, are obvious by comparing the three images.

$$u = \frac{x - Tx - (z - Tz)\tan\theta}{S} \tag{1}$$

and

$$v = f\cos\theta\frac{y - Ty}{z - Tz} + p_v \tag{2}$$

Note that the pushbroom scanning system has parallel projection in the *u* direction (Eq. (1)), but has perspective geometry in the *v* direction (Eq. (2)). Figure 2 shows three real gamma-ray images, with three different scanning angles – zero, ten and twenty degrees, respectively. Each image has a size of 621x256 pixels, i.e., 621 scans of the 256-pixel linear images.

3. γ-RAY LINEAR PUSHBROOM STEREO

A dual-scanning system is a *linear pushbroom stereovision system*. It can be constructed with two approaches: two linear pushbroom scanning sensors with different scanning angles, or a single scanning sensor to scan the same cargo twice with two different scanning directions. For a 3D point *(x,y,z)*, its image correspondences in the stereo pair can be represented by

$$\begin{aligned} u_k &= \frac{x - T_{xk} - (z - T_{zk})\tan\theta_k}{S_k} \\ v_k &= f_k\cos\theta_k\frac{y - T_{yk}}{z - T_{zk}} + p_{vk} \end{aligned} \qquad (k=1, 2) \tag{3}$$

Therefore the depth of the point can be recovered as

$$z = \frac{d - d_0}{\tan\theta_1 - \tan\theta_2} \tag{4}$$

where

$$d = S_2u_2 - S_1u_1 \tag{5}$$

is the *visual displacement* (measured in feet) of the point (*x, y, z*) measured in the pair of stereo images, and

$$d_0 = (T_{x1} - T_{z1}\tan\theta_1) - (T_{x2} - T_{z2}\tan\theta_2)$$

is the fixed offset between two images. In Figure 2, the visual displacements, particularly the back surface of the cargo container, are obvious by comparing these three images. Note that Eq. (4) is acquired by only using the *u* coordinates of the stereo images (Eq. (5)). Further, the depth of any point is proportional to its visual displacement in the stereo pair, therefore the depth resolution is independent of depth.

After the depth is obtained via the pushbroom stereo, the *x* and *y* coordinates of the point can be calculated from one of the two images, for example

$$\begin{aligned} x &= u_1S_1 + z\tan\theta_1 + T_{x1} - T_{z1}\tan\theta_1 \\ y &= \frac{(v_1 - p_{v1})(z - T_{z1})}{f_1\cos\theta_1} + T_{y1} \end{aligned} \tag{6}$$

4. SENSOR CALIBRATION

In order to use two scanning systems to calculate 3D information, we need to calibrate each scanning the system first. For each scanning setting, the following parameters are required for 3D estimation: the focal length f, the image center p_v, the scanning angle θ, the scanning speech S, and the initial sensor location (T_x, T_y, T_z). In order to fulfill this task, we need to know a set of 3D points $\{(x_i, y_i, z_i)\}$ and their corresponding image points $\{(u_i, v_i)\}$, i=1, 2,…, N. Our calibration method only needs to know the dimension of the container, which is

length(x)*height(y)*depth(z)=20*8*8 (ft^3).

in the example of Figure 2. Then we locate the 8 vertices of the rectangular container (refer to Figure 1) in each gamma-ray image by manually picking up the 8 corresponding image points.

An interesting property of the linear pushbroom sensor is that Eq. (1) and Eq. (2) can work independently. Therefore, in calibrating the sensor, we first obtain the "parallel projection parameters" in Eq. (1) and then the "perspective projection parameters" in Eq. (2). Eq. (1) can be turned into a linear equation with three unknowns, i.e., S, $\tan\theta$ and T_x-$T_z\tan\theta$:

$$u_i S + z_i \tan\theta + (T_x - T_z \tan\theta) = x_i \tag{7}$$

Given more than three pairs of points (i=1, 2,..., N where $N \geq 3$)., we can solve the linear system to find the three unknowns by using the least square method. Similarly, Eq. (2) leads to a linear equation with five unknowns, i.e. f, fT_y, p_v, p_vT_z and T_z:

$$(y_i \cos\theta) f - \cos\theta(fT_y) + z_i p_v - (p_v T_z) + v_i T_z = v_i z_i \tag{8}$$

With the known θ and given more than five pairs of points (i=1, 2,..., N where $N \geq 5$), we can solve the linear equation system. Note that from Eq. (7) we can only find the values of the speed S and the angle θ and a combined parameter T_x-$T_z\tan\theta$. Nevertheless, this is sufficient for obtaining the depths of points using Eq. (4). Table 1 shows the results of the "parallel parameters" for all the three settings corresponding to images a, b, and c in Figure 2. All the rest of the parameters, including Tx, can be obtained after solving Eq. (8), in order to calculate the x and y coordinates of 3D points by using Eq. (6). Table 2 shows the "perspective parameters" and the T_x values for all the three settings.

Table 3 shows the 3D measurements using the *image* point pairs used for calibration between two views, the ten-degree and the twenty-degree images. The purpose is to examine the accuracy of the pushbroom stereo modeling and calibration results. The numbers of the points listed in Table 3 are labeled in Figure 1 for comparison. For the container with a dimension of 20x8x8 ft^3, the average errors in depth z, length x and height y are 0.064 ft, 0.033 ft and 0.178 ft respectively, indicating that the pushbroom modeling and calibration is accurate enough for 3D measurements. Note that the accuracy of the estimation in Table 3 only reflects the errors in sensor modeling and calibration. No image localization errors are included. The depth error δz introduced by image localization error δu can be estimated as the first derivative of z with respect to u using Eqs. (3) and (4), that is

$$\delta z = \frac{S}{\tan\theta_1 - \tan\theta_2}\delta d \tag{9}$$

In Eq. (9) we assume that two scans share the same speed (i.e. $s_1 = s_2 \triangleq s$), which are almost true for our example in Figure 2 (see Table 1). In this example, one-pixel image localization error introduces an error of 0.254 ft in depth estimation, using the parameters listed in Table 1. We have three notes about the calibrations results.

(1) The parallel parameters estimation: the estimated speeds for scanning the three images are almost the same (S = 0.0456-0.0458), and the angles obtained are very close to the parameters provided by SAIC, i.e., 0, 10 and 20 degrees.

(2) The perspective parameters estimation: the three sets of parameters, including the focal lengths, the image centers, and the camera initial locations are consistent with each other.

(3) The parallel parameters are more accurate than the perspective ones due to fewer parameters in calibration and no inter-dependency among unknowns in the former, whereas three of the five unknowns in Eq. (8) are not independent, thus creating larger errors in the estimations of the y coordinates than the x coordinates (Table 3). In solving Eq. (8) using SVD, we found that the one of the four singular values of the matrix $\mathbf{A}^T\mathbf{A}$ is almost zero, where $\mathbf{A}$ is the coefficient matrix of the linear system of Eq. (8). Therefore, the pseudo inverse of matrix $\mathbf{A}^T\mathbf{A}$ was used.

Table 1. Parallel projection parameters

Img	*S (ft/pixel)*	$\tan\theta$	θ *(degrees)*	T_x-$T_z\tan\theta$
a	0.04584	0.00143	0.0821	-7.398
b	0.04566	0.16552	9.3986	-7.283
c	0.04561	0.34493	19.031	-7.309

Table 2. Perspective projection parameters

Img	*F (pxl)*	T_y *(ft)*	p_v*(pxl)*	p_vT_z	T_z *(ft)*	T_x*(ft)*
a	427.78	-0.41558	21.148	-177.78	-14.815	-7.419
b	441.24	-0.42881	17.787	-191.78	-15.141	-9.789
c	456.18	-0.41037	19.250	-198.03	-15.000	-12.48

Table 3. 3D measurements of the test points

No	*X*	*Y*	*Z*	*dX*	*dY*	*dZ*
0	-0.033	-0.179	-0.063	-0.033	-0.179	-0.063
1	20.033	-0.177	0.063	0.033	-0.177	0.063
2	19.967	-0.152	7.936	-0.033	-0.152	0.064
3	0.033	-0.204	8.064	0.033	-0.204	0.064
4	-0.033	7.787	-0.063	-0.033	-0.213	-0.063
5	20.033	7.856	0.063	0.033	-0.144	0.063
6	19.967	7.799	7.936	-0.033	-0.201	0.064
7	0.033	7.844	8.064	0.033	-0.156	0.064

5. STEREO MATCHING AND 3D VISUALIZATION

5.1. Automatic stereo matching

The gamma-ray images in cargo inspection are similar to those X-ray images generated by a medical imaging system. Therefore registration techniques using in medical images[11,16] could be employed for our application. We adapt a free-form deformation registration method[11] for our gamma-ray stereo matching. There are several advantages of this method. First, it is automatic: it is a voxel based registration method (i.e., pixel based in our case of 2D images) so it does not require any feature extraction and can be done fully automatically. Second, it is fast: it is capable to find local deformation, i.e., the displacement field for each voxel (pixel), and hence a global minimization can be conducted efficiently via calculus of variations[8,16].

The free-form deformable registration problem[11] is described as finding the displacement field of an image that minimizes an energy function. The energy function is composed of not only the similarity of intensities of two images, but also the smoothness of the displacement field.

Let A(**u**) be the reference image and B(**u**) be the target image, the displacement is defined as a mapping from the domain A to the domain B:

$$\mathbf{d_u} : \mathrm{A} \rightarrow \mathrm{B} \tag{10}$$

So that a point $\mathbf{u} = (u_1, u_2) = (u, v)$ in the reference image moves to $\mathbf{u} + \mathbf{d_u(u)}$ in the target image. The energy function is defined as

$$\varepsilon(\mathbf{d_u}) = \int_{\mathbf{u}\in\Omega^2} \left[R^2(\mathbf{u}, \mathbf{d_u}) + \lambda \sum_{i=1}^{2} \sum_{j=1}^{2} \left(e_{ij}\right)^2 \right] d\mathbf{u} \tag{11}$$

Here $R(\mathbf{u}, \mathbf{d_u}) = B(\mathbf{u} + \mathbf{d_u}) - A(\mathbf{u})$ is the residual between the two images, λ is a constant weight, and $e_{ij} \equiv \dfrac{\partial d_{u_i}}{\partial u_j}$ $(i = 1,2; j = 1,2)$ is the partial derivative of the displacement vector which describes how smooth the movement is around a pixel.

The method tries to minimize the difference of the intensity while maintains the smoothness of the displacement fields at the same time. We can see that when R^2 is small, the energy is dominated by summation of the squares of the partial derivatives of the displacement vector, yielding a slowly varying field.

Since the energy function is a function of variables **u,** $\mathbf{d_u}$ and $\dfrac{\partial \mathbf{d_u}}{\partial \mathbf{u}}$, by using the calculus of variations[8,16], the displacement field can be found by solving the following Euler-Lagrange equation,

$$\lambda \nabla^2 \mathbf{d_u} - R(\mathbf{u}, \mathbf{d_u}) \frac{\partial R(\mathbf{u}, \mathbf{d_u})}{\partial \mathbf{d_u}} = 0 \tag{12}$$

where $\dfrac{\partial R(\mathbf{u}, \mathbf{d_u})}{\partial \mathbf{d_u}}$ is the gradient vector field of the deformed image. Then a finite difference scheme is used to solve this nonlinear elliptic partial differential equation, and Newton iteration is applied to update the displacement at each iteration, as

$$d_{u\kappa}^{new} = d_{u\kappa}^{old} + \frac{L_\kappa^{old}}{\lambda + (g_\kappa^{old})^2}, \kappa = 1,2 \tag{13}$$

Here $L_\kappa = \lambda \nabla^2 d_{u\kappa} - [B(\mathbf{u} + \mathbf{d_u}) - A(\mathbf{u})] g_\kappa(\mathbf{u} + \mathbf{d_u})$, and g_κ is the gradient in the κ's dimension $(\kappa = 1,2)$ of the image B at location $\mathbf{u} + \mathbf{d_u}$.

Multi-resolution technique is applied in our implementation. It can be viewed as a systematic way for structuring local information into global information in order to deal with the gamma-ray images that lack salient visual features. Using a multi-resolution technique also overcomes the limitation of a one-resolution approach in handling large displacements using the free-form deformable registration method. In the multi-resolution registration, large displacements can be found computationally efficiently at coarse level, even with low accuracy, which is later refined with the finer resolution calculation.

Four layers of image resolutions are used in our implementation: 621x256, 310x128, 155x64 and 77x32. From coarsest level to the finest resolution, the number of iterations to find the displacements at each level are 128, 64, 32 and 16,

respectively. After registration at a lower level is done, the displacements at this level then are up-sampled and scaled to the next higher resolution level and to be used as the initial displacements for that level.

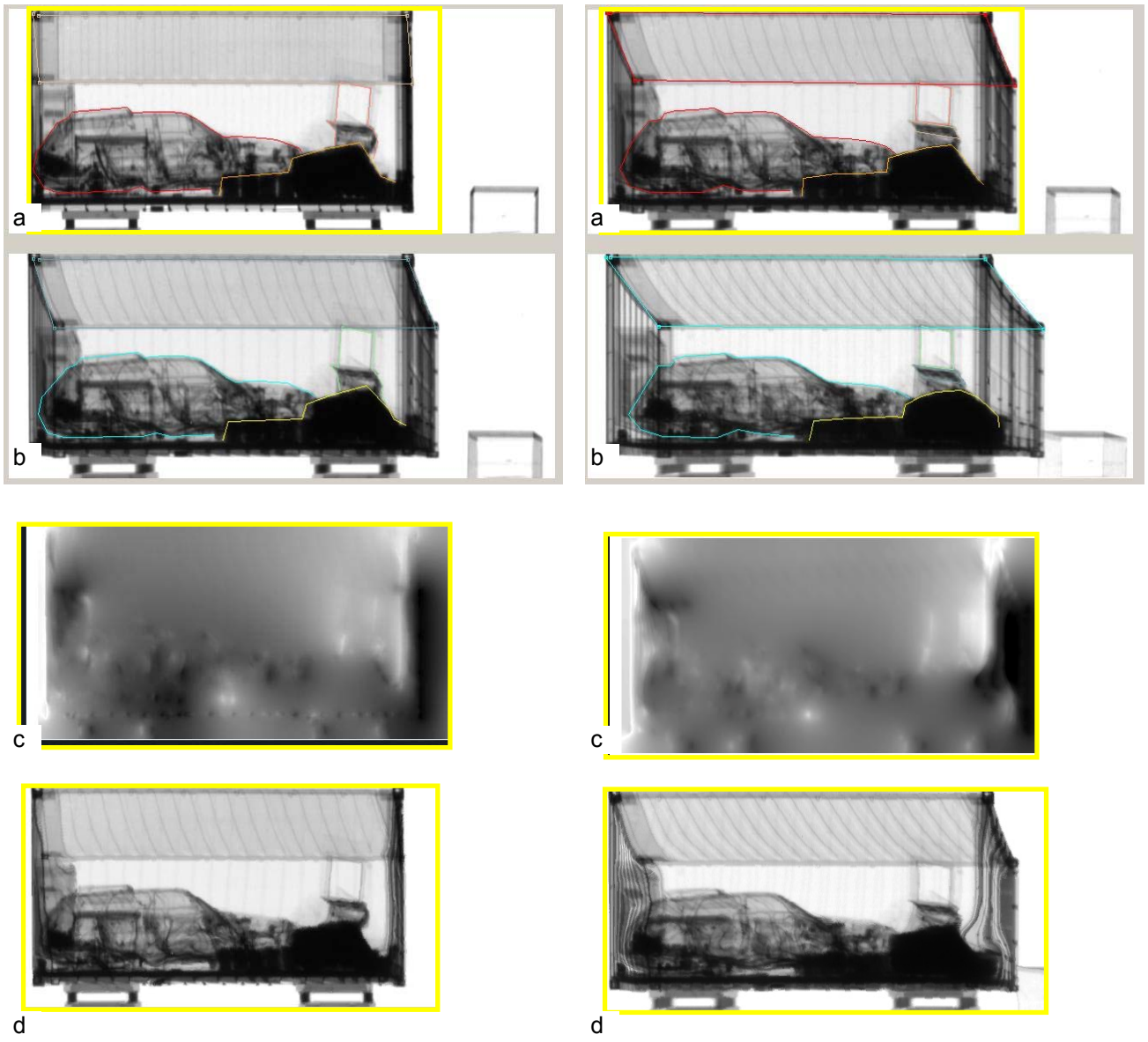

(1) The pair of zero- and ten-degree images **(2) The pair of the ten- and twenty-degree images**

Figure 3. Pushbroom stereo matching. In each of columns (1) and (2): (a) reference image A(u), (b) target image B(u), (c) "depth" map of the selected window (shown in yellow in a), and (d) the target image warped to reference image, $B(u+d_u)$. In the two depth maps, invert offsets are shown, i.e., the brighter points are closer to the sensor. The corresponding pairs of contours that are interactive selected are shown in (a) and (b).

We also utilize the epipolar geometry constraint of the pushbroom stereo system in our matching algorithm. In a stereo imaging system, the displacement vector of a point should be on the point's epipolar line. The epipolar lines of a stereo pair from the linear pushdown stereo scanning system are approximately horizontal scanlines (i.e., $v_1 \approx v_2$ in Eq. 3). Thus in the multi-resolution registration process, we limit the displacement vector to be one-dimensional in the horizontal direction (i.e., along the x-axis) at all levels except the finest resolution level. At the finest resolution level, we allow offset of +2/-2 pixels at the vertical direction (i.e., along the y-axis) to account for geometric errors in sensor setup and sensor calibration.

The whole registration process takes less than 10 seconds on a Pentium-M 1.5GHz laptop. Once it is done, the displacement vectors for all points on the reference image are obtained. Since we have displacement vectors for each point on the image, we can generate a "depth" map for a stereo pair. Figure 3 shows the stereo matching results for two pairs of gamma-ray images, the pair of the zero- and ten-degree images, and the pair of the ten- and twenty-degree images. Since the depth z of the point is proportional to the offset (d in Eq. 5 and d_u in Eq. 10) along the x-axis, we directly use d_u for showing the depth map (Figure 3c). Areas with high contrasts (such as object boundaries) have more accurate matching results, whereas areas with less contrast turn to have smaller offsets in the estimated results. In addition, since the algorithm also smoothes out the displacements in the global minimization process, the depth maps turn to be smooth. Figure 3d shows the results of warping the target images to the corresponding reference images using the estimated displacement vector fields. The performance of the stereo matching algorithm, particularly at locations with sufficient contrasts, can be seen by comparing Figure 3a and Figure 3d.

After the depth map of a stereo pair is generated, our interactive program allows us to pick up lists of points in a reference image, and show the contour along these points in the reference image and the contour along the corresponding points in the target image, side by side. In Figure 3a and Figure 3b, the pairs of colored contours show the accuracy of those points on the boundaries of objects – the roof of the cargo container, and three objects inside the container. Note that those correspondence points are found automatically by our stereo matching algorithm.

Studying the gamma-ray/X-Ray imaging principle will be helpful in better understanding the problem in stereo matching. Penetration of gamma-ray /X-ray can be described by the following equation:

$$I^{out} = I^{in} e^{-\mu dx} \tag{14}$$

where I is the energy strength and μ is the attenuation of the material the ray pass through and dx is the distance that between the point the ray goes in and the point the ray goes out. The penetration of X-ray energy is exponential decay with distance and attenuation. Thus the resulting intensity for a single point that the detector received from the two scans of different angles would vary. Therefore our stereo matching algorithm works better at those points on the boundaries of unblocked objects since the attenuation of the materials the rays pass through would be consistent between two different views.

5.2. 3D estimation and visualization

We have also developed a 3D measurement and visualization procedure for measuring and visualizing those objects in interests. The reconstructed 3D structures of those contour points that are picked up by a user in the stereo matching stage are rendered as wire frames in 3D. For each set of points that are selected for 3D measurements and visualization, a connected 3D line-frame representation is generated. Figure 4 shows several views of the 3D frame representation of the four point sets obtained in Figure 3 for the stereo pair of the ten- and twenty-degree images. The black rectangular frame is the reconstruction of the cargo container using the calibration image data. The red line frames are generated from the 3D measurements by the automated stereo match algorithm. It is clearly shown that the automated stereo matches provide very good 3D measurements for the cargo container and the objects inside.

With the 3D visualization, 3D measurements of sizes and shapes, for example, are made simple by using the most convenient views. Further object measurements and identification will be our future work.

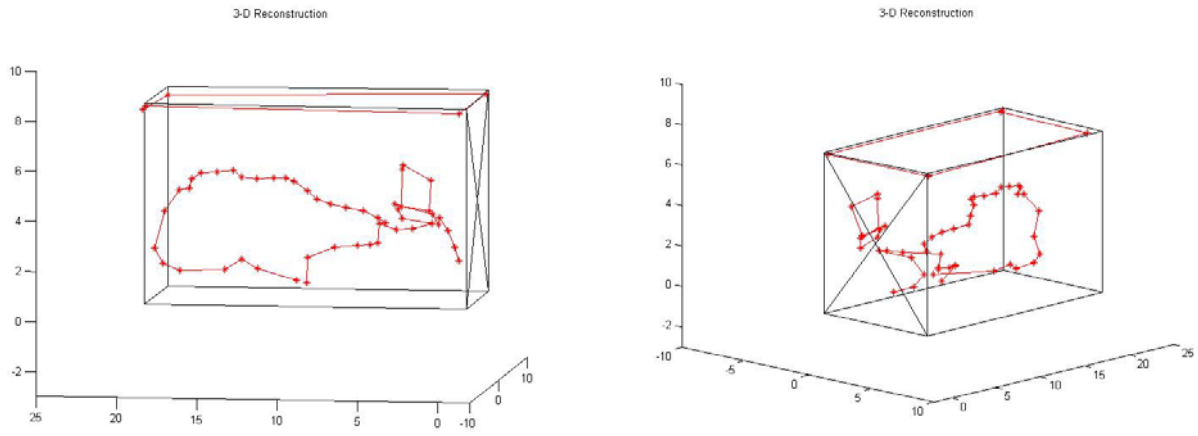

(a) View 1 **(b) View 2**

Figure 4. 3D measurements and visualization of objects inside the cargo container. The black rectangular frames show the cargo container constructed from the test data in Table 3. The red lines (with stars) show the 3D estimates from automated stereo matches, for the cargo container and three objects inside.

6. CONCLUSIONS AND DISCUSSIONS

In this paper we present a practical approach for 3D measurements in gamma-ray (or X-ray) cargo inspection. The linear pushbroom sensor model is used for the gamma-ray scanning system. Thanks to the constraints of the real scanning system, we model the system by using a linear pushbroom model with only one rotation angle instead of three. This greatly simplifies the calibration procedure and increases the robustness of the parameter estimation. Using only the knowledge of the dimensions of the cargo container, we can automatically calibrate the sensor and find all the sensor parameters, including the image center, the focal length, the 3D sensor starting location, the viewing direction, and the scanning speed. The sensor modeling and calibration is accurate enough for 3D measurements.

Then, a fast and automated stereo matching algorithm based on the free-form deformable registration approach is proposed to obtain 3D measurements of objects inside the cargo. With both the automatic matching procedure and the interactive 3D visualization procedure, we hope that the 3D measurements for cargo inspection could be put into practical use.

We have made the first attempt to use pushbroom stereo for 3D gamma-ray/x-ray cargo inspection. We want to pursue this research in two directions. First, we are actively seeking collaboration with cargo inspection vendors to implement more tests on real data in real deployments. By doing this we will obtain much important information that was not available when doing the current experiments, e.g. the real parameters of the sensor setting, the ground truth data of the objects under inspection. Second, we will continue our study on gamma-ray stereo matching algorithms. Most of the algorithms in literature of stereo vision work well only for normal visible images. We have tried the deformable registration method originally developed for medical imaging applications to this new application. However, more work needs to be done to obtain dense and more accurate 3D information, particularly for small, concealed 3D objects. The knowledge of physics and optics in generating the radiographic images could be very helpful in advancing this direction of research.

ACKNOWLEDGEMENTS

This work is partially supported by the Air Force Research Laboratory (AFRL) under the RASER Program (Award No. FA8650-05-1-1853) and an Human Effectiveness Program (Award No. F33615-03-1-63-83), by Army Research Office (ARO) under Award No. W911NF-05-1-0011, and by the CUNY Graduate Research Technology Initiative (GRTI) program. We thank Dr. Rex Richardson and Dr. Victor J. Orphan at Science Applications International Corporation (SAIC) for providing us gamma-ray images and the dimension data of the cargo container. Thanks are also given to Li Zhao at the City College of New York for implementing the calibration algorithm in Section 4.

REFERENCES

1. Chai, J. and H –Y. Shum, 2000. Parallel projections for stereo reconstruction. In *Proc. CVPR'00*: II 493-500.
2. Dickson, P., J. Li, Z. Zhu, A. Hanson,, E. Riseman, H. Sabrin, H. Schultz and G. Whitten, 2002. Mosaic generation for under-vehicle inspection. *IEEE Workshop on Applications of Computer Vision*, Orlando, Florida, Dec 3-4, 2002
3. Gupta, R. and R. Hartley, 1997. Linear pushbroom cameras, *IEEE Trans PAMI*, 19(9), Sep. 1997: 963-975
4. Gupta, R., A. Noble, R. Hartley, J. Mundy, A. Schmitz, 1995. Camera calibration for 2.5-D X-ray metrology. In *Proc. ICIP'95*, Vol. 3, Oct 23 - 26, 1995 Washington D.C.
5. Hardin, W., 2002. Cargo Inspection: Imaging Solutions Wait for Government's Call, Machine Vision Online, Dec 2002.
6. Hardin, W., 2004. US Seaports: Finding the Needle in Hundreds of Haystacks, Machine Vision Online, June 2004.
7. Hitachi, 2004. Cargo container X-ray inspection systems, *Hitachi Review*, 53(2) June 2004: 97-102. http://www.hitachi.com/rev/field/industriasystems/2006638_12876.html
8. Keener, J. P., Principles of Applied Mathematics: Transformation and Approximation, Reading, MA: Addison-Wesley, 1998.
9. Klette, R., G. Gimel'farb, R. Reulke, 2001. Wide-angle image acquisition, analysis and visualization. Proc. 14th Internat. Conf. ``Vision Interface" (VI'2001), Ottawa, Canada, June 2001, 114-125.
10. Koschan,A., D. Page, J.-C. Ng, M. Abidi, D. Gorsich, and G. Gerhart, 2004. SAFER under vehicle inspection through video mosaic building," *International Journal of Industrial Robot*, September 2004, 31(5): 435-442.
11. Lu, W., M. L. Chen, G. H. Olivera, K. J. Ruchala, TR Mackie. Fast free-form deformable registration via calculus of variations. *Physics in Medicine and Biology*, (49) June 2004, pp 3067-3087
12. Noble, A., R. Hartley, J. Mundy and J. Farley. X-Ray Metrology for Quality Assurance, In *Proc IEEE ICRA'94*, vol 2, pp 1113-1119
13. Peleg S, M, Ben-Ezra and Y. Pritch, 2001. Omnistereo: panoramic stereo imaging, *IEEE Trans. PAMI*, 23(3): 279-290.
14. Shum, H.-Y. and R. Szeliski, 1999. Stereo reconstruction from multiperspective panoramas. In *Proc. ICCV'99*: 14-21
15. Orphan, V. J., R. Richardson and D. W. Bowlin, 2002. VACIS™ – a safe, reliable and cost- effective cargo inspection technology, *Port Technology International*, p. 61-65. www.porttechnology.org/journals/ed16/section02.shtml
16. Xu, C., Deformable models with application to human cerebral cortex reconstruction in magnetic resonance images. PhD Thesis, John Hopkins University, 2000.
17. Zheng, J. Y., and S. Tsuji, 1992. Panoramic representation for route recognition by a mobile robot. *International Journal of Computer Vision*, 9(1), 1992: 55-76.
18. Zhu, Z. and A. R. Hanson, 2004. LAMP: 3D Layered, Adaptive-resolution and Multi-perspective Panorama - a New Scene Representation, *Computer Vision and Image Understanding*, 96(3), Dec 2004, pp 294-326.
19. Zhu, Z. , E. M. Riseman and A. R. Hanson, 2001. Parallel-perspective stereo mosaics. In *Proc. ICCV'01*, vol I: 345-352.
20. Zhu, Z., E. M. Riseman, A. R. Hanson, 2004. Generalized Parallel-Perspective Stereo Mosaics from Airborne Videos, *IEEE Trans PAMI*, 26(2), Feb 2004, pp 226-237